Analysis of the effect of different punch shapes on thickness distribution of AA5052 sheet in stretch flanging process

Surendra Kumar
Sanjay Kumar Panthi (sanjay_panthi@yahoo.co.in)
AMPRI: Advanced Materials and Processes Research Institute CSIR
Meraj Ahmed
Manoj Soni
Manjeet Singh Hora

Research Article

Keywords: Stretch flanging process, FEM, Thickness/thinning distribution, Strain distribution, Friction coefficient, Punch profile

Posted Date: March 3rd, 2022

DOI: https://doi.org/10.21203/rs.3.rs-1323947/v1

Abstract

Flanging is a well-known process in sheet metal forming (SMF) process, which is highly used in automobile industry and in manufacturing of home appliances. The effectiveness of the flanging process depends on the geometry of tools, material properties etc. In the present research assessment, influence of punch shape on thickness variation in aluminium alloy sheet in stretch flanging (SF) process is presented, which is major challenge of this process. Six types of punches are used in the present work i.e. spherical, conical, cylindrical, 2 step, 3 step and 6 step. Punch of shape is an important part of tooling that affects the deformation behaviour of blank. FEM simulation work is carried out for the assessment of thickness and strain distribution in the flange portion (along the die profile radius and midsection (centre) of blank) in stretch flanging process. The results are validated with experiments that observed in a very good agreement. The reduction in thickness of blank is found minimum in hemispherical punch along the die profile radius and in the midsection of blank as compared to other punch geometry. Thus, it is concluded from this work, based on the reduction of thickness of blank, that the hemispherical punch profile is more suitable in the product design by stretch flanging process.

1. Introduction

Flanging is one types of bending process, which is mostly used to manufacture automotive and aerospace components [1]. It is mainly used to apply rigidity and smoothness to the parts and also used to assemble various products [1–5]. Straight, stretch and shrink flanging are three types of flanging process [6]. They are indicated in Fig. 1. In stretch flanging, one edge portion of the blank is fixed and opposite edge of blank is remains free to bend by 90^0 to form a flange [1, 4]. If the arc length of the final flange is more than the original length then it is called a stretch flanging (SF) process. It is indicated in Fig. 1 **(b, c and d)**. It occurs due to stretching of materials in the circumferential direction [3]. The tension found largest at the edge of die profile radius whereas it is minimum at top and midsection of the flange [3]. Shrink flanging process is opposite to stretch flanging process. In shrink flanging process, material is compressed in the circumferential direction which is illustrated in Fig. 1 (**e** and **f**). In SFP, circumferential strain is a main parameter that causes fracture in the flange. In this process, cracks occurs when circumferential strain reaches at the certain limit [3, 5]. Necking, thinning, localized cracks/fracture (Fig. 1 **(d)**) etc. are the main types of failure in this case [3]. These failures can be forecast and minimize with the support of finite element simulation. The finite element simulation is an important numerical tool that is capable in predicting necking, crack initiation and its location, strain distribution, forming load and thickness variation. It also saves the time in designing and cost of component as compared to experimental procedure due to fast optimization of parameters involved in the process [7–9].

In the past decade, several researchers have attempted to forecast and analyse the failure mechanism in the different sheet metal forming (SMF) process using FE analysis. Feng et al analysed the effects of various sheet geometrical parameters on the formability of flange in the curved SF process through simulation [2]. P. Hu et al generated couple of analytical models for shrink and stretch flanging processes for calculation of blank size [6]. Yogesh Dewang et al carried out the experimental and numerical

simulation work for the analysis of binder force effect in stretch flanging of AA5052 sheet [10]. G. Ellen et al created the analytical model for the evaluation of circumferential strain and proposed a semi-empirical failure criteria for analysis of wrinkling in shrink flanging process [11]. Sriram and Chintamani worked on stretch flanging (SF) process to analyse the effect of geometrical parameters on AHSS Steel sheet. It was found that the flange angle is a main parameter for the same process [12]. Cliff Butcher et al predicted the formability in SF process using models of lower bound (Sun-Tvergaard-Needleman) and upper bound (GTN) damage in FEM simulation [13]. Vafaeesefat and Khanahmadlu validated the numerical results with experimental one in stretch z-flange forming process which was based on shell-elements [14]. Several researchers had been studied the effect of different materials on stretch-flangeability [15, 16]. Thinning, fracture, wrinkling etc. were studied in deep drawing process by researchers [17–21]. D. Li et al created the mathematical model for the axisymmetric case and studied the influenc of parameter like sheet and its geometry in V-shape SF process. It was found that the geometrical parameters were more dominated than the materials parameters [22]. Y. Dewang et al investigated stretch flanging (SF) process to see effect of initial flange length, friction coefficient, profile radius of die and punch, gap between punch and die for the prediction of edge crack location and its propagation using FE simulation and it was also justified with experimental result [23].

In the current era, several researchers have been used different punch profiles and different techniques to enhance the formability of material and also found the effect of these on failures (thinning, necking, localized cracks etc.) in various sheet metal forming processes such as deep drawing, shrink, stretch and hole flanging. Yohei Abe et al improved the formability and minimize the fracture in UHSS steel sheet in SF process using punch gradually that contacts and mitigated the tensile stress [24]. Tong Wen et al used the bar tool with tapered shoulder for analysis of flexible and versatile (stretch and shrink) flanging process in ISMF technology and measured the wall thickness distribution [25]. Surendra K. et al investigated the effect of various punch profiles on aluminium alloy AA5052 blank in SF process. It was found that the minimum crack length can be achieved with in hemispherical/conical punch shape with respect to other shapes [26]. L I Jun-chao et al predicted the mechanical properties and distribution of thickness in blank in the incremental deep drawing process by numerical simulation [27]. Suresh kurra et al performed the experimental and FE simulation for the assessment of formability and thickness distribution in ISMF process using a varying wall angle conical frustum [28]. Yuung-Ming H. used the elasto-plastic FE code for the analysis of the effect of the web width, the flange height and the punch corner radius for prediction of distribution of thickness in SF process [29]. Fracz et al studied the effect of 3 punch profile (i.e. conical, hemispherical and flat) on distribution of thickness in hole flanging process and found that the uniform thickness distribution in the case of flat bottomed punch profile [30]. P. Sarkulvanich et al used three types of punches (conical, flat and spherical punch) to evaluate the influence of blank edge of AHSS steel sheet using FE analysis in SF (hole) process [31]. Zein et al predicted the effect of springback and thinning in deep drawing process [32]. Krawczyk et al performed the hole expansion test, with 3 types of punches (i.e. conical, spherical and cylindrical) and used with 4 types of steels workpiece. Enhancement in the diameter of holes were observed maximum in the case of spherical punch profile is used [33]. Rongjing Zhang et al analysed the effect of spring back and thinning

on multilayer sheet metal forming using the hydro-mechanical deep drawing process [34]. Surendra k. et al analysed the influence of geometrical parameters on thinning and crack behaviour of AA5052 sheet in SF process [35]. G. Ingarao et al investigated the influence of thinning and springback of dual-phase steels in U- shape bending operation which was based on multi-objective approach [36]. B. Sarkar et al analysed the influence of materials parameters on thinning distribution in SMF process and determined that the thinning variation is the function of strain path [37]. B.T. Tang et al optimized the design of blank and predicted the distribution of thickness in deep drawing process of square box and clover-shaped cup using enhanced inverse analysis method [38].

It is observed from the literature that a very less focused has been given, by the past researchers, on the influence of different punch geometry on deformation of sheet in stretch/curved flanging process, which is extensively used in different sectors such as aerospace, automotive industries and household applications. The deformation behaviour/mode in sheet depends on types of contact and area of contact between the surfaces of sheet and punch in SF process.

Non-uniform distribution of thickness and localized cracking are some of the big challenges in SMF process as well as in SF process. To minimize the blank thinning and cracks in SF process, different punch profile tools like cylindrical, 2 step, 3 step, 6 step, conical and hemispherical punch are used in the present research. Influences of these punch profiles have been performed in order to understand the deformation behaviour of blank in the SF process using FEM software ABAQUS/Explicit. Thickness distribution (its location) in blank is predicted along the midsection and the die profile radius and evaluated the contact behaviour/mode of blank with punch at different displacement percentage of punch. Experiments have been conducted on a hydraulic press machine to justify the FEM results.

2. Material And Methods

2.1 Mechanical properties of material

Aluminum alloy AA5052 sheet was used as blank to perform the present research work. It is broadly used in the manufacturing of structural components of aerospace and automobiles sectors. Mechanical properties of materials have been evaluated using a UTM machine as per E8 (ASTM) standard [39, 40]. Fig. 2 indicates the stress-strain curve for the AA5052 material. The value of density, Poisson's ratio and Young's modulus of material are 2680kg/m^3, 0.33 and 70.3GPa, respectively [26, 35, 41]. These material properties are used for the purpose of FE simulate.

2.2 FE modelling and simulation

FE model was created to analysis the deformation behaviour of AA5052 sheet for prediction the thinning and load distribution in SF process using finite element software ABAQUS/Explicit. Fig. 3 shows the FEM model used in the present research. In this work, six different kinds of punches were used i.e., hemispherical, conical, cylindrical, two step, three step and six step and Fig. 4 illustrated the details of all punch profiles. The height and radius of die were 60 mm and 35mm respectively, and the top surface of

die was designed similar to the bottom surface of blank-holder for the uniform distribution of load onto the sheet. The blank-holder, punch and die are meshed with element R3D4 which acted as a rigid body in FEM.

Sheet metal blank of thickness 0.5 mm, width 40 mm, and length 120 mm was taken in the present study to perform the experimentation of SF process. A CAD model corresponding to same geometry was generated and meshed with C3D8R-element (deformable and slave surfaces). It was also meshed S4R shell-type element for the assessment of thickness distribution for different punch profiles in SF process. The surface of S4R type elements was considered as a slave surface in the simulation. S4R is a four noded three-dimensional stress and displacement shell type element with reduced integration. It has total six degrees of freedom at each node. The blank was kept between the blank-holer and die. 0.1mm clearance is provided between the bottom surface of the blank-holder and top surface of sheet, and top surface of die and bottom surface of blank for the minimization of the penetration of the blank [42]. All the constraints were implemented at the reference node in the rigid part. Die location and direction were fixed like a stationary body while the punch displacement was allowed to move only in the z-direction (downward) for the formation of flange in all cases of FEM analysis. The gap 1mm is taken between the punch and die and friction coefficient between the interfaces is assumed to be 0.1 [22]. In the SF process, initially, one edge portion of blank (80 mm) is placed between the blank-holder and die while other edge portion (opposite to initial edge portion) of the blank is kept free for formation of flange. Thereafter, the blank is finally developed similar to shape of the die profile/geometry. FEM work is executed for all punch profiles and data were recorded in the form of thickness distribution.

2.3 Experimental procedure

To justify the FEM results, experiments were executed on hydraulic press machine of capacity 50 kN (Blank ram 20 kN + Primary ram30 kN). Primary ram and blank ram are used for holding (clamping) the punch and to apply the force onto the blank-holder for binding the blank between the blank-holder and die respectively. The tooling consists of blank-holder, die, punch and blank as indicated in Fig. 5. Various geometries of punch are indicated in Fig. 6. Dimensions of the punch, blank-holder, die and blank were kept similar to the FEM simulation and it was used for validation purpose. Punch was held on primary ram and die was rigidly fixed on working table of the machine by tightening the bolt. Blank positioning was similar to FEM procedure. The primary ram was moved with 1 mm/s constant velocity to generate the flange. Thereafter load was release and the sample was taken out for the measurement of the thickness distribution at different location in the flange portion of the blank. In the experimental work, only three punch i.e., cylindrical, conical and hemispherical were used in SF process for the validation of FE simulation results.

3. Analysis Of Bending Force

Maximum bending force to form the flange can be analysed by the following equation [4, 43]

$$\mathbf{Maximumbendingforce(F)} = \left(\frac{\mathbf{K_{bf} * (TS) * W * t^2}}{\mathbf{D}} \right)$$

1

Where, K_{bf} is the constant. The value of K_{bf} dependent for types of bending process. It is 0.33 and 0.7 for edge and U type bending respectively.

D = Span length (die opening)

T_s (TS) = Materials strength (Tensile)

t = Blank thickness

W = Blank width

The value of W, t, D, UTS, K_{bf}, coefficient of friction between the tool interface, tool set-up geometry affect the requirement of maximum bending force [26]. Therefore, from the Fig. 7 & 8 it can be observed that the span length is due to change in punch profile that it affects the contact location between the punch profile and sheet. Decreasing order of the span length variation for different punch geometries are: hemispherical ≥ conical > stepped like punch > cylindrical [26]. Die opening length is generally inversely proportional to the maximum bending force which can be seen from equation (1). Therefore, the maximum bending force is highly depends on punch profile and contact between the blank and tools and it is shown in Fig. 8 and in equation (1) [4, 26, 43]. It is clear from the Fig. 7 and 8 that the contact area between punch and blank for different punch shapes varies at with respect to percentages of total punch displacement. It is due to the slope of the punch that varies for various punch geometry. It can be say from Fig. 7 and Fig. 8 that the minimum punch load is required in hemispherical punch while maximum in cylindrical punch profile according to equation (1) [4, 43]. It may be due to the very slow or sudden contact take place between the tools i.e. punch and blank.

4. Results And Discussion

4.1 Justification of simulation results

Punch profile is an important part of tooling that influnces the deformation behaviour of blank in SF process. A evaluation of results in the form of terms of length of crack, crack shape in flange and thickness distribution along the die profile radius and at the midsection (center) in the flange for cylindrical, conical and hemispherical punch profiles are shown in Fig. 9 to Fig. 12. The half section view of final shape and zoom portion of stretch flange with crack shape and location for cylindrical, conical and hemispherical punch profiles are also shown in figure 9. It is observed from the Fig. 9, the crack initiates along path-1 (center) and propagates towards to the sheet centre. The maximum impression was

noticed when cylindrical punch was used whereas it is minimum for hemispherical punch. Thinning and thickening of blank may be varies due to impression of punch on the deformed blank.

A column (2 & 3) and columns (4 & 5) indicates the FEM and experimental results, respectively. These results are illustrated in Fig. 9. The length of crack is measured for three cases. It has been plot as a bar graph which is shown in Fig. 10. In simulation and experimental length of cracks are measured by using a digital Vernier calipers and query information tool, respectively. The length of crack and its shape in simulation are found very similar to the experimental one.

So it can be conclude from experimental and FEM results that crack length depends on geometry of punch. If the contact curvature of the geometry of punch is uniform with blank, it supports in creating a uniform contact with blank. Due to this, uniform distribution of stress occurred in the blank during deformation. Minimum crack was found in hemispherical punch which has a more uniform curvature/slope as compared to cylindrical and conical punch profiles.

In this study, the influence of different punch shapes i.e. hemispherical, conical, cylindrical, 6 step, 3 step and 2 step on deformation behaviour of blank punch were studied in stretch flanging operation. All six punch shapes were taken in FE simulation and three shape considered to conduct the experiments in order to validate the FEM results. The influence of punch profile is presented in the form of thickness distribution in the deformed flange. The results taken from FE simulation and experimental results are found in a good support to each other with respect to thickness distribution along the **path-1** and **path-2** of the deformed blank. Thickness distribution in the sheet metal blank was calculated by defining the **path – 1** and **path – 2** in the deformed sheet metal blank that is selected along the die profile radius and along the midsection of blank respectively as shown in Fig. 11. Starting points is mentioned in the **path – 1** and **path – 2** for assessment of thickness distribution in deformed blank which is shown in Fig. 11. Fig. 12 and 13 represents the plots between the flange thickness variation and distance from the free side of edge to the blank center (**path-1**). It is revealed from the Fig. 12 that the minimum thinning in flange is observed in the case of hemispherical punch whereas it is found maximum in cylindrical punch profile case by FE simulation as well as by experimental one. Fig. 14 and 15 shows the graph between the flange thickness variation and distance from the midsection of free edge lower side up-to top portion of deformed flange (**path-2**). It is clear from the Fig. 14 that the minimum thinning is observed in the case of hemispherical punch whereas it is found maximum in cylindrical punch profile. Fig. 12 and Fig. 14 represents the evaluation of results of simulation and experimental which is found in very good agreement.

Table 1 shows the maximum thinning and thickening in sheet for different punch profile. Fig. 16 shows the contour plots of thickness variation in flange and its location in the deformed blank to evaluate the effect of different punch profile by FE simulation. Fig. 16 illustrated the thinning location and thicker location in the formed flange. In cylindrical punch profile, final thickness and thickening were found 0.3703 mm and 0.5375 mm respectively. The final thickness of 0.3801, 0.3817 and 0.3791 mm were found in two step, three step and six step punch respectively, whereas final thickening of 0.5494 mm,

0.5483 mm and 0.5547 were observed for the same punch profile. The final thickness and thickening were observed 0.3882 mm and 0.5684 mm respectively in case of a conical punch profile. The final thickening and thickness were found 0.6406 mm and 0.3909 mm respectively in hemispherical punch profile. These numerical values were found from the contours as shown in Fig. 16. It is disclosed from the Fig. 16 and **Table 1**, the maximum thickening and minimum thinning are observed in the case of hemispherical punch whereas minimum thickening and maximum thinning in case of cylindrical punch profile. It is concluded from the Fig. 12 to Fig. 16 the hemispherical punch profile is better than the other punch profiles (i.e. two step, three step, six step, cylindrical and conical) in terms of thinning/thickness distribution in the deformed flange (along the path-1 and path-2) (along the die profile radius and midsection direction) and minimum crack length in blank along the path-1.

4.2 Circumferential and radial strain

The influence of geometry of punch can be represented in the form of strain distribution during the SF process. Nature of circumferential is tensile whereas radial strain is compressive. Strain distribution in deformed blank is predicted by defining a meridian **path 1** and **2**. It is indicated in Fig. 11. Fig. 17 and 18 represents the plots between the strains with respect to distance along the die profile radius up-to sheet center as mentioned in the Fig. 11 (**path-1).** Maximum circumferential strain is observed near to the side edge of flange (i.e. edge corner of die profile radius) while minimum it is noticed at midsection of blank. It is clearly seen from the Fig. 17 and 18. Minimum circumferential and radial strain are observed in the profile of hemispherical punch as compared to other shapes of punch. Fig. 19 and 20 shows the graph between the strain and distance from the midsection of free edge lower side up-to-top portion of deformed flange as shown in Fig. 11 (**Path-2**). Variation of circumferential strain is less as compared to radial strain when considered the **path-2**. It is clear from the Fig. 19 and 20, that the influence of punch profile is more on radial strain distribution in the midsection of flange (**path-2**) as compared to edge corner of die profile radius of deformed blank. Circumferential strain is more dominate at the place of side edge of flange (i.e. edge corner of die profile radius) whereas radial strain is more effective at the place of around the midsection of deformed flange. It is observed from the Fig. 17 to 20, that Circumferential and radial strain distributions are minimum in hemispherical punch profile while these are maximum in cylindrical punch (step punch) profile. Circumferential and radial strain distributions are varying with changes in the geometries of punch profiles. Therefore, it can say that effects of radial and circumferential strain distribution on thickness variation in deformed blank due to the slope of geometry of punch and contact between the punch profile and blank.

4.3 Effect of coefficient of friction

Figure 21 shows the contour plots of variation of thickness (thinning and thickening) and its location in the deformed blank to found out the effect of friction coefficient (i.e. μ = 0.05, 0.10, 0.15 and 0.20) on deformation of sheet and it is carried out only for hemispherical punch profile by FE simulation. Final thickness of 0.3950, 0.3909, 0.3853 and 0.33801 mm were found at different coefficient of friction 0.05, 0.1, 0.15 and 0.2 are considered in hemispherical punch profile case, respectively, whereas final thickening of 0.6506 mm, 0.6486 mm, 0.6268 and 0.6193 were found for the same set of coefficient of

friction. **Table 2** shows the maximum thinning and thickening of sheet occurs for different coefficient of friction. It is concluded from the Figure 21 and **Table 2**, the thinning and thickening is decreasing with increase the friction coefficient for the same cases (punch geometry) [44, 45], because materials flow of sheet was restricted by friction force and deformation of materials are also found more when friction coefficient is considered high.

5. Conclusions

In the present research, influence of different punch profiles on the deformation behaviour of aluminium alloy AA5052 blank in SF process is studied. FE simulation results have been verified with an experimental one in term of length of crack and distribution of thickness that are noticed in a very good agreement. The minimum forming load may be required for the hemispherical punch geometry as compared to that of other profile of punch considered in the present research [26]. It is because of the effect of contact behaviour between the punch and blank. The maximum thickening and minimum thinning in blank and minimum crack length in deformed flange are found in case of hemispherical punch profile. The minimum thinning (minimum reduction of thickness in the blank) is observed in the case of a hemispherical punch profile whereas it is obtained maximum in case of cylindrical punch profile is used. The maximum thickening in blank is decreased with increasing the **μ** whereas the maximum thinning is decreased with increasing the **μ** for the same punch profile, because materials flow of sheet was restricted by friction force and deformation of materials are also found more when friction coefficient is considered high. Hence hemispherical punch profile is more suitable in the products by the SF process on the bases of thinning, thickening and crack length.

Declarations

Acknowledgments:

We would like to thank Director, Council of Scientific and Industrial Research (CSIR) - AMPRI, Bhopal, India for providing the facility and support for carrying out the present research.

Declaration of conflicting interests/competing interests:

The author(s) declared no potential conflicts of interest with respect to the research, authorship, and/or publication of this article.

Author contribution:

Surendra Kumar: contributed in development of methodology, performed experiments and FEM simulation and analysed results; Dr. S. K. Panthi: conceptualized the proposed work and provided resources for experimental and simulation and supervised the work; Dr. Meraj Ahmed: suggested inputs for simulation and literature review; Manoj Soni: contributed in preparation of samples, editing and

writing paper; **Manjeet Singh Hora:** contributed in finite element simulation and review/editing manuscript.

Funding: Not applicable

Data and materials availability: The data and supporting materials of the results of present work are available within the article. Data will be made available when requested.

Code availability: Not applicable

Ethics approval and consent to participate There is no ethical issue in the present work. Yes, there is consent from all authors to participate.

Consent to participate: The authors agree to participate in the article

Consent for publication: All co-authors declare their consent for publication of this work.

References

1. Chuan-Tao W, Kinzel G, Altan T (1995) Failure and wrinkling criteria and mathematical modeling of shrink and stretch flanging operations in sheet-metal forming. J. Mater. Proc. Technol. 53(3): 759-780. https://doi.org/10.1016/0924-0136(94)01766-T
2. Feng X, Zhongqin L, Shuhui L, Weili (2004) Study on the influences of geometrical parameters on the formability of stretch curved flanging by numerical simulation. J. Mater. Proc. Technol. 145(1): 93-98. https://doi.org/:10.1016/S0924-0136(03)00866-5
3. Asnafı N (1999) On stretch and shrink flanging of sheuminium by fluid forming. J. Mater. Proc. Technol. 96(1): 198–214. https://doi.org/10.1016/S0924-0136(99)00352-0
4. Kalpakjian S, Sekar K, Vijai, Schmid SR (2014) Manufacturing engineering and technology, Pearson
5. Wang N-M, Wenner M (1974) An analytical and experimental study of stretch flanging. Int J Mech Sci 16(2):135–143
6. Hu P, Li D, Li Y (2003) Analytical models of stretch and shrink flanging. Int J Mach Tools Manuf 43(13):1367–1373. https://doi.org/10.1016/S0890-6955(03)00150-0
7. Logan DL (2011) A first course in the finite element method. Cengage Learning, Boston
8. Panthi S, Ramakrishnan N, Pathak K, Chouhan J (2007) An analysis of springback in sheet metal bending using finite element method (FEM). J. Mater. Proc. Technol. 186(1): 120-124. https://doi.org/10.1016/j.jmatprotec.2006.12.026
9. Panthi S, Ramakrishnan N, Ahmed M, Singh SS, Goel M (2010) Finite element analysis of sheet metal bending process to predict the springback. Mater Des 31(2):657–662. 10.1016/j.matdes.2009.08.022
10. Dewang Y, Panthi SK, Hora M (2019) Binder force effect on stretch flange forming of aluminum alloy. Mater Manuf Processes 34(13):1516–1527. https://doi.org/10.1080/10426914.2019.1655154

11. Zhang GE, Yao J, Hu SJ, Wu X (2003) Shrink flanging with surface contours. J Manuf Processe 5(2):143–153
12. Sriram S, Chintamani J (2005) Guidelines for stretch flanging advanced high strength steels. AIP Conference Proceedings, AIP. pp. 681-686
13. Butcher C, Chen Z, Worswick M (2006) A lower bound damage-based finite element simulation of stretch flange forming of Al–Mg alloys. Int J Fract 142(3–4):289–298. https://doi.org/10.1007/s10704-006-9044-3
14. Vafaeesefat A, Khanahmadlu M (2011) Comparison of the numerical and experimental results of the sheet metal flange forming based on shell-elements types. Int J Precis Eng Manuf 12(5):857–863. https://doi.org/10.1007/s12541-011-0114-8
15. Chun EJ, Do H, Kim S, Nam D-G, Park Y-H, Kang N (2013) Effect of nanocarbides and interphase hardness deviation on stretch-flangeability in 998 MPa hot-rolled steels. Mater Chem Phys 140(1):307–315
16. Lee J, Lee S-J, De BC (2012) Cooman, Effect of micro-alloying elements on the stretch-flangeability of dual phase steel. Mater Sci Eng : A 536:231–238. https://doi.org/10.1016/j.msea.2012.01.003
17. Dougall J, Mc, Stevenson M, McKeever K (2005) Analysis of sheet steel fracture during deep drawing. J Fail Anal Prev 5(5):20–25. https://doi.org/10.1361/154770205X65972
18. Pantazopoulos G, Sampani A (2006) Failure analysis of fractured deep-drawn 1050 aluminum circles. J Fail Anal Prev 6(3):24–28. https://doi.org/10.1361/154770206X107307
19. Gupta R, Kumar VA, Karthikeyan M, Ramkumar P, Narayanan PR, Sinha P (2010) Investigation of cracks generated in Columbium alloy (C-103) sheets during deep drawing operation. J Fail Anal Prev 10(3):228–232. https://doi.org/10.1007/s11668-010-9341-z
20. Wu J, Zou F (2016) Deep drawing failure map of a coated metal sheet based on the process parameters. J Fail Anal Prev 16(3):361–368. https://doi.org/10.1007/s11668-016-0097-y
21. Kumbhar SV (2018) Pressure Optimization and Failure Prediction for Deep Drawing Process of Sheet Metal Products: A Case Study. J Fail Anal Prev 18(4):948–956. https://doi.org/10.1007/s11668-018-0485-6
22. Li D, Luo Y, Peng Y, Hu P (2007) The numerical and analytical study on stretch flanging of V-shaped sheet metal. J. Mater. Proc. Technol. 189(1): 262-267. https://doi.org/10.1016/j.jmatprotec.2007.01.035
23. Dewang Y, Hora M, Panthi S (2015) Prediction of crack location and propagation in stretch flanging process of aluminum alloy AA-5052 sheet using FEM simulation. Trans Nonferrous Met Soc China 25(7):2308–2320. https://doi.org/10.1016/S1003-6326(15)63846-8
24. Abe Y, Mori K-i, Norita K (2013) Gradually contacting punch for improving stretch flangeability of ultra-high strength steel sheets. CIRP Ann Manuf Technol 62(1):263–266. http://dx.doi.org/10.1016/j.cirp.2013.03.059
25. Wen T, Zhang S, Zheng J, Huang Q, Liu Q (2015) Bi-directional dieless incremental flanging of sheet metals using a bar tool with tapered shoulders. J. Mater. Proc. Technol. 229: 795-803.

http://dx.doi.org/10.1016/j.jmatprotec.2015.11.005

26. Kumar S, Ahmed M, Panthi S (2020) Effect of punch profile on deformation behaviour of AA5052 sheet in stretch flanging process. Arch Civ Mech Eng 20:18. https://doi.org/10.1007/s43452-020-00016-2
27. LI J-c, Chong L, Zhou T-g (2012) Thickness distribution and mechanical property of sheet metal incremental forming based on numerical simulation. Trans Nonferrous Met Soc China 22:s54–s60. https://doi.org/10.1016/S1003-6326(12)61683-5
28. Kurra S, Regalla SP (2014) Experimental and numerical studies on formability of extra-deep drawing steel in incremental sheet metal forming. J. Mater. Proc. Technol. 3(2): 158-171. http://dx.doi.org/10.1016/j.jmrt.2014.03.009
29. Huang Y-M (2007) An elasto-plastic finite element analysis of the sheet metal stretch flanging process. Int J Adv Manuf Technol 34(7–8):641–648. https://doi.org/10.1007/s00170-007-0958-3
30. Frącz W, Stachowicz F, Trzepieciński T (2012) Investigations of thickness distribution in hole expanding of thin steel sheets. Arch Civ Mech Eng 12(3):279–283. http://dx.doi.org/10.1016/j.acme.2012.06.006
31. Sartkulvanich P, Kroenauer B, Golle R, Konieczny A, Altan T (2010) Finite element analysis of the effect of blanked edge quality upon stretch flanging of AHSS. CIRP Ann Manuf Technol 59(1):279–282. https://doi.org/10.1016/j.cirp.2010.03.108
32. Zein H, Sherbiny M, El, Abd-Rabou M (2014) Thinning and spring back prediction of sheet metal in the deep drawing process. Mater Des 53:797–808. http://dx.doi.org/10.1016/j.matdes.2013.07.078
33. Krawczyk J, Gronostajski Z, Polak S, Jaśkiewicz K, Chorzępa W, Pęcak I (2016) The influence of the punch shape and the cutting method on the limit strain in the hole expansion test. Key Engineering Materials, Trans Tech Publ. pp. 129-137. https://doi.org/10.4028/www.scientific.net/KEM.716.129
34. Zhang R, Lang L, Zafar R, Lin L, Zhang W (2016) Investigation into thinning and spring back of multilayer metal forming using hydro-mechanical deep drawing (HMDD) for lightweight parts. Int J Adv Manuf Technol 82(5–8):817–826. DOI 10.1007/s00170-015-7415-5
35. Kumar S, Ahmed M, Panthi S (2020) Investigation on the Crack and Thinning Behavior of Aluminum Alloy 5052 Sheet in Stretch Flanging Process. J Fail Anal Prev 20(4):1212–1228. https://doi.org/10.1007/s11668-020-00922-w
36. Ingarao G, Lorenzo R, Di, Micari F (2009) Analysis of stamping performances of dual phase steels: a multi-objective approach to reduce springback and thinning failure. Mater Des 30(10):4421–4433. https://doi.org/10.1016/j.matdes.2009.04.001
37. Sarkar B, Jha B, Mukerjee D, Jha S, Narasimhan K (2002) Thinning as a failure criterion during sheet metal forming. Practical Fail Anal 2(2):63–64
38. Tang B, Zhao Z, Lu X, Wang Z, Zhao X, Chen S (2007) Fast thickness prediction and blank design in sheet metal forming based on an enhanced inverse analysis method. Int J Mech Sci 49(9):1018–1028. https://doi.org/10.1016/j.ijmecsci.2007.02.003
39. Davis JR (2004)Tensile testing, ASM international

40. ASTM E (2001) Standard test methods for tension testing of metallic materials, Annual book of ASTM standards. ASTM
41. Ahmed M, Kumar DR, Nabi M (2017) Enhancement of formability of AA5052 alloy sheets by electrohydraulic forming process. J Mater Eng Perform 26(1):439–452. https://doi.org/10.1007/s11665-016-2446-0
42. Documentation A (2013) Getting started with Abaqus interactive edition, Version
43. Groover MP (2007) Fundamentals of modern manufacturing: materials processes, and systems. John Wiley & Sons
44. Padmanabhan R, Oliveira MC, Alves JL, Menezes LF (2007) "Influence of process parameters on the deep drawing of stainless steel". Finite Elem Anal Des 43:1062–1067. https://doi.org/10.1016/j.finel.2007.06.011
45. Zein H, El SM, Abd-Rabou M (2014) "Thinning and spring back prediction of sheet metal in the deep drawing process". Mater Des 53:797–808. http://dx.doi.org/10.1016/j.matdes.2013.07.078

Tables

Table – 1. The maximum thinning and thickening in blank of different punch profile on deformed flange by FE simulation

S. No.	Profile of the punch	Initial thickness of blank (mm)	Maximum thinning in blank (mm)	Maximum thickening in bank (mm)
1	Cylindrical	0.5	0.1297	0.0375
2	Two stepped	0.5	0.1199	0.0494
3	Three stepped	0.5	0.1183	0.0483
4	Six stepped	0.5	0.1209	0.0547
5	Conical	0.5	0.1118	0.0684
6	Hemispherical	0.5	0.1091	0.1406

Table – 2. The maximum thinning and thickening in blank of hemispherical punch profile with different coefficient of friction on deformed flange by FE simulation

S. No.	Coefficient of friction (μ)	Initial thickness of blank (mm)	Maximum thinning in blank (mm)	Maximum thickening in bank (mm)
1	μ = 0.05	0.5	0.105	0.1506
2	μ = 0.10	0.5	0.1091	0.1406
3	μ = 0.15	0.5	0.1147	0.1268
4	μ = 0.20	0.5	0.1199	0.1193

Figures

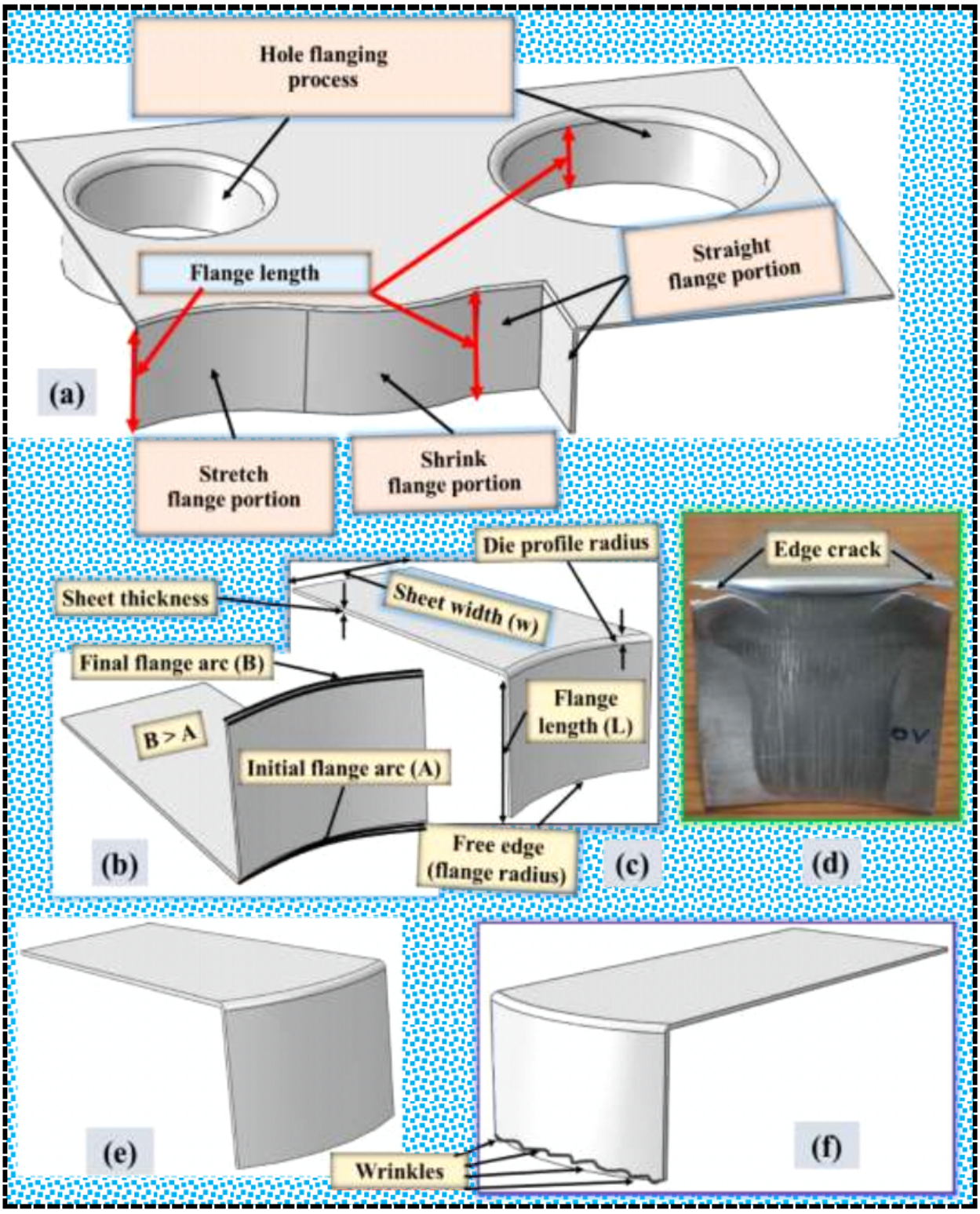

Figure 1

Different flanging processes (a) Complex flanges, (b, c and d) stretch flanges and (e and f) Shrink flanges

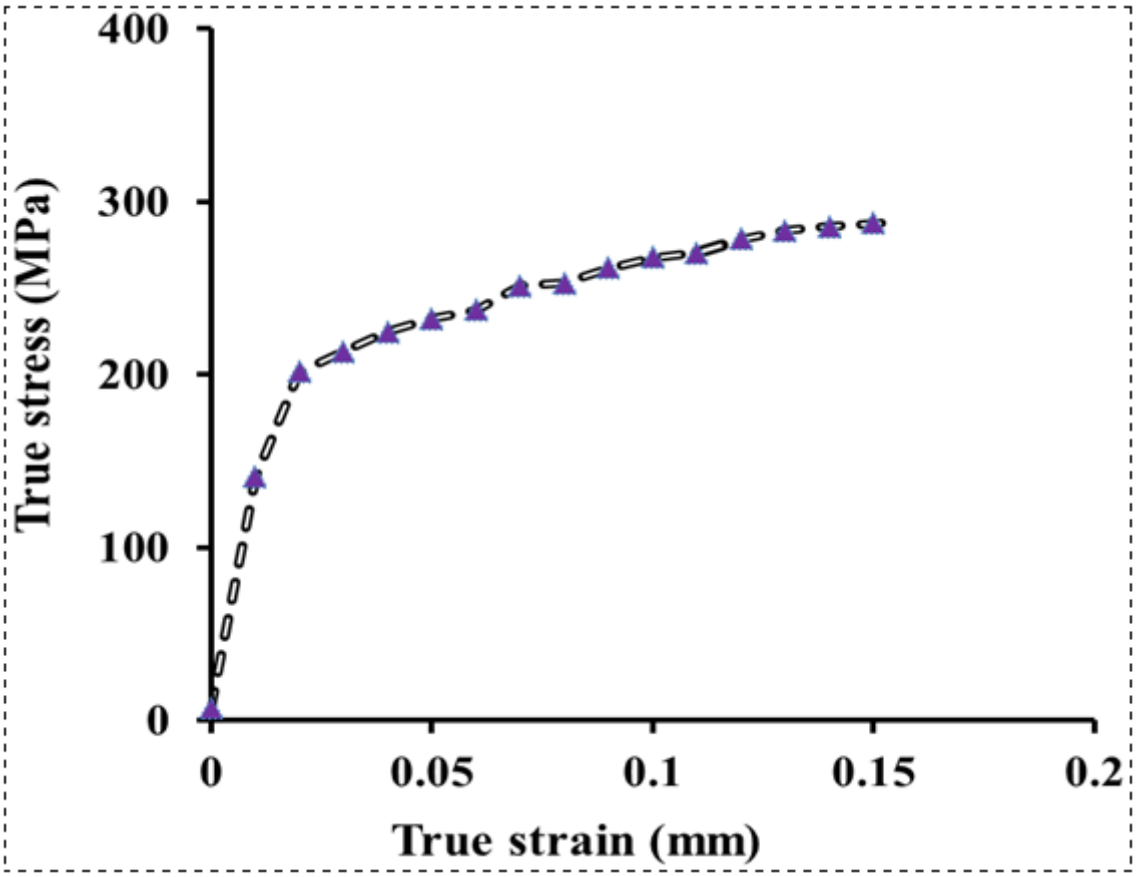

Figure 2

Flow stress-strain curve

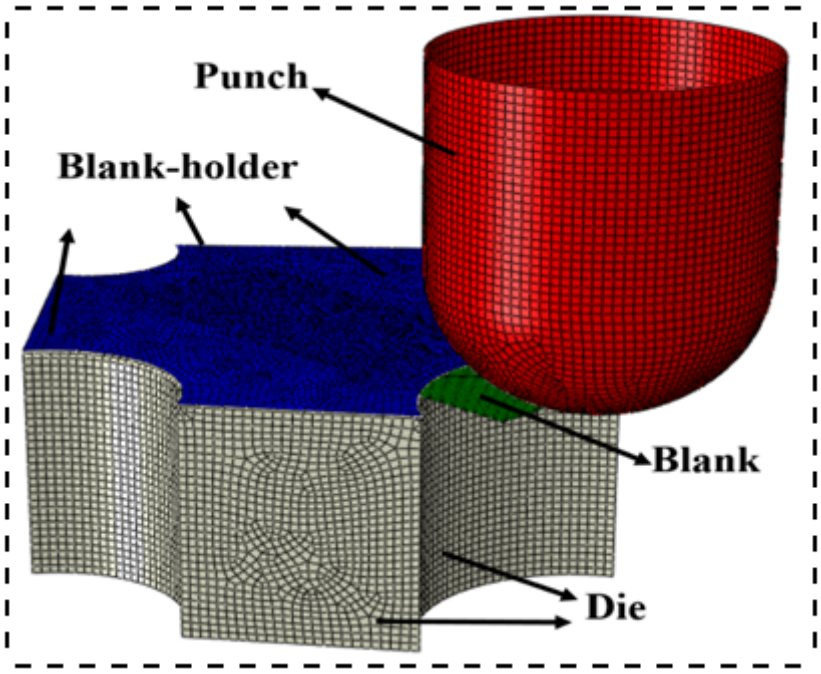

Figure 3

FEM model for SF process

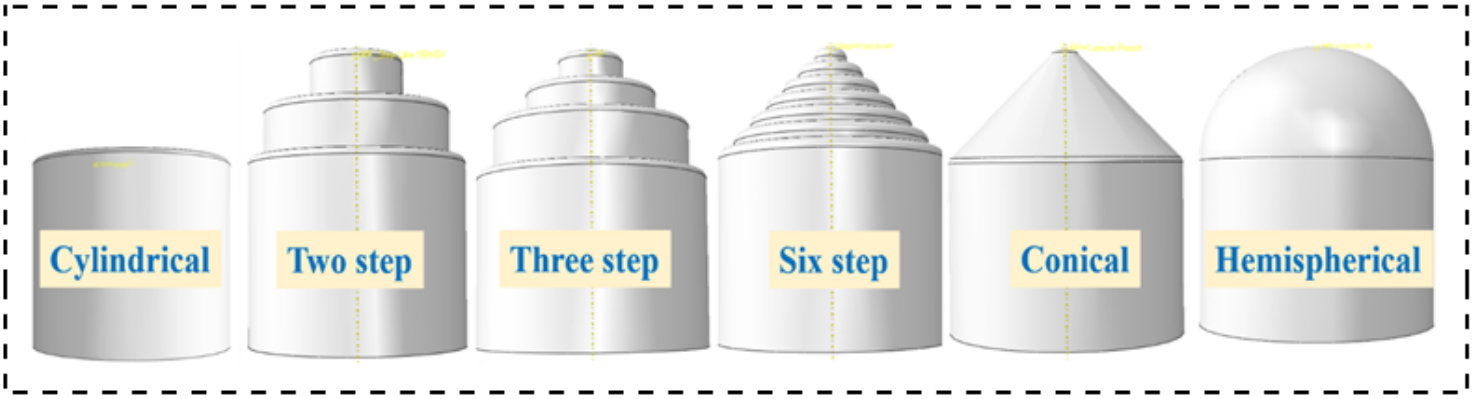

Figure 4

CAD model of six punch profiles i.e. cylindrical, 2 step, 3 step punch, 6 step punch were used for SF process

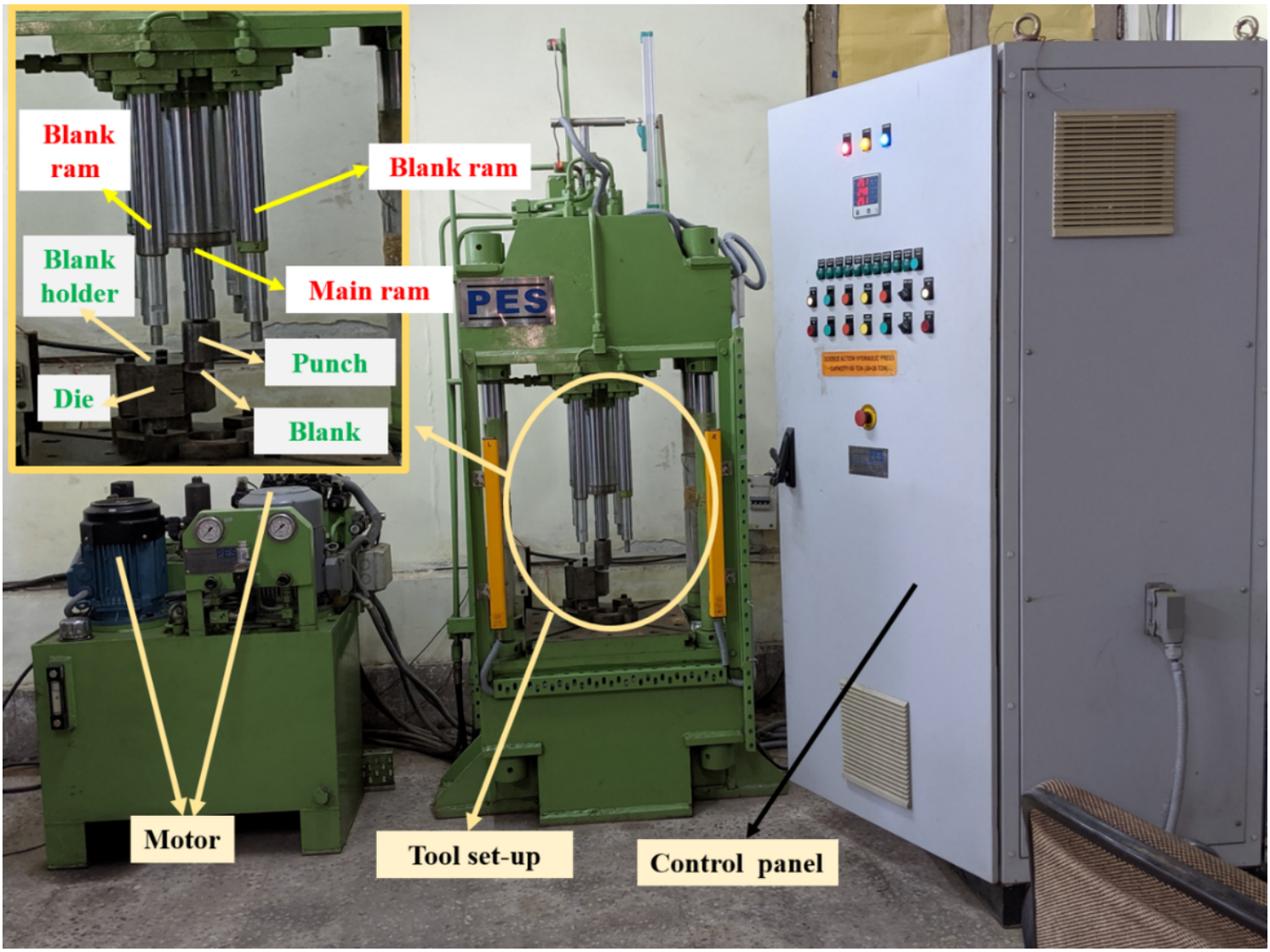

Figure 5

Experimental tooling step-up for stretch flanging (SF) process

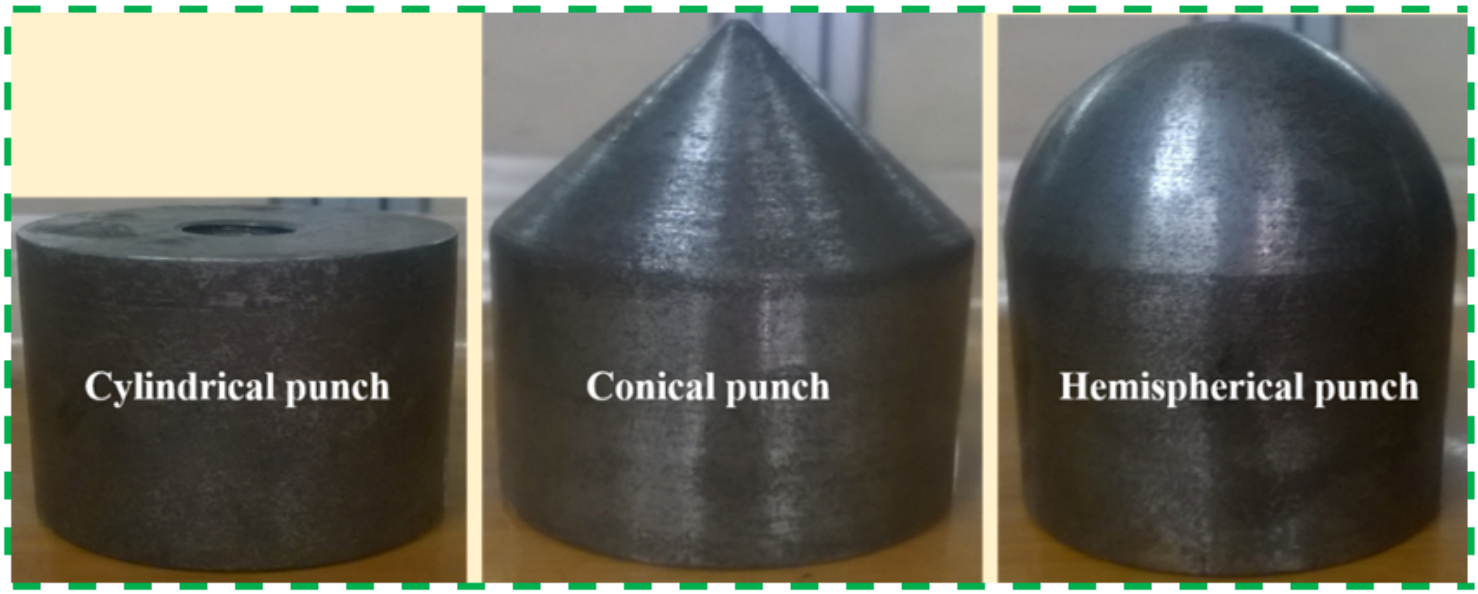

Figure 6

Three punch profiles i.e. cylindrical, conical and hemispherical punch were used for the experimental work

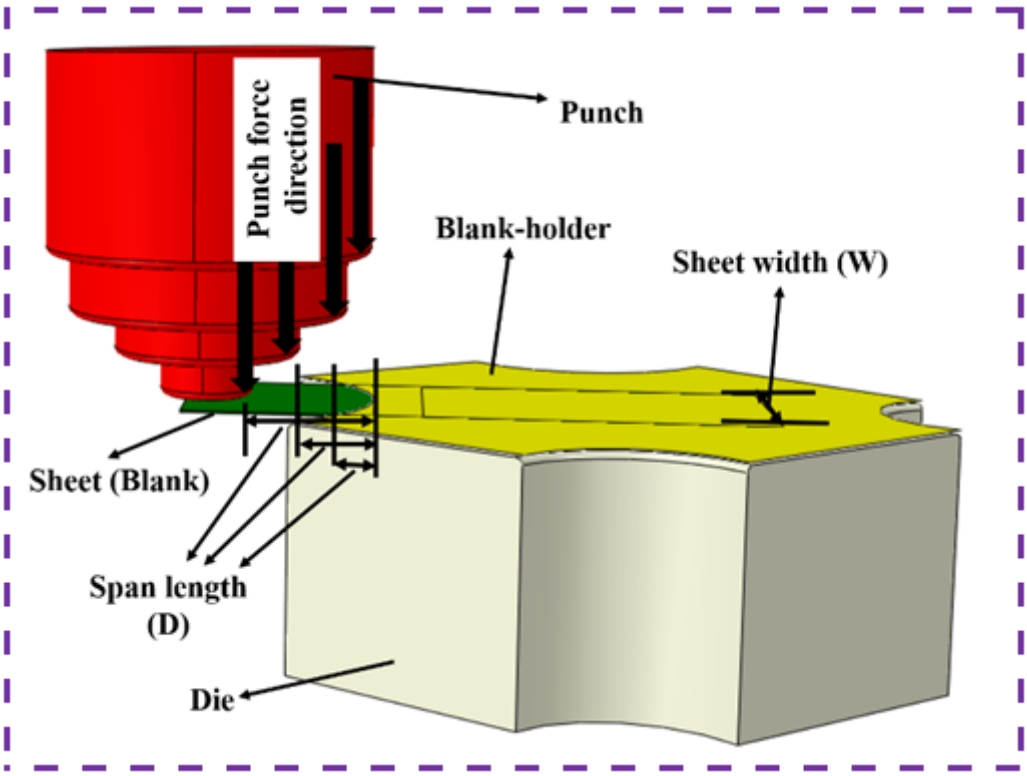

Figure 7

CAD model of analysis of bending force in stretch flanging (SF) process

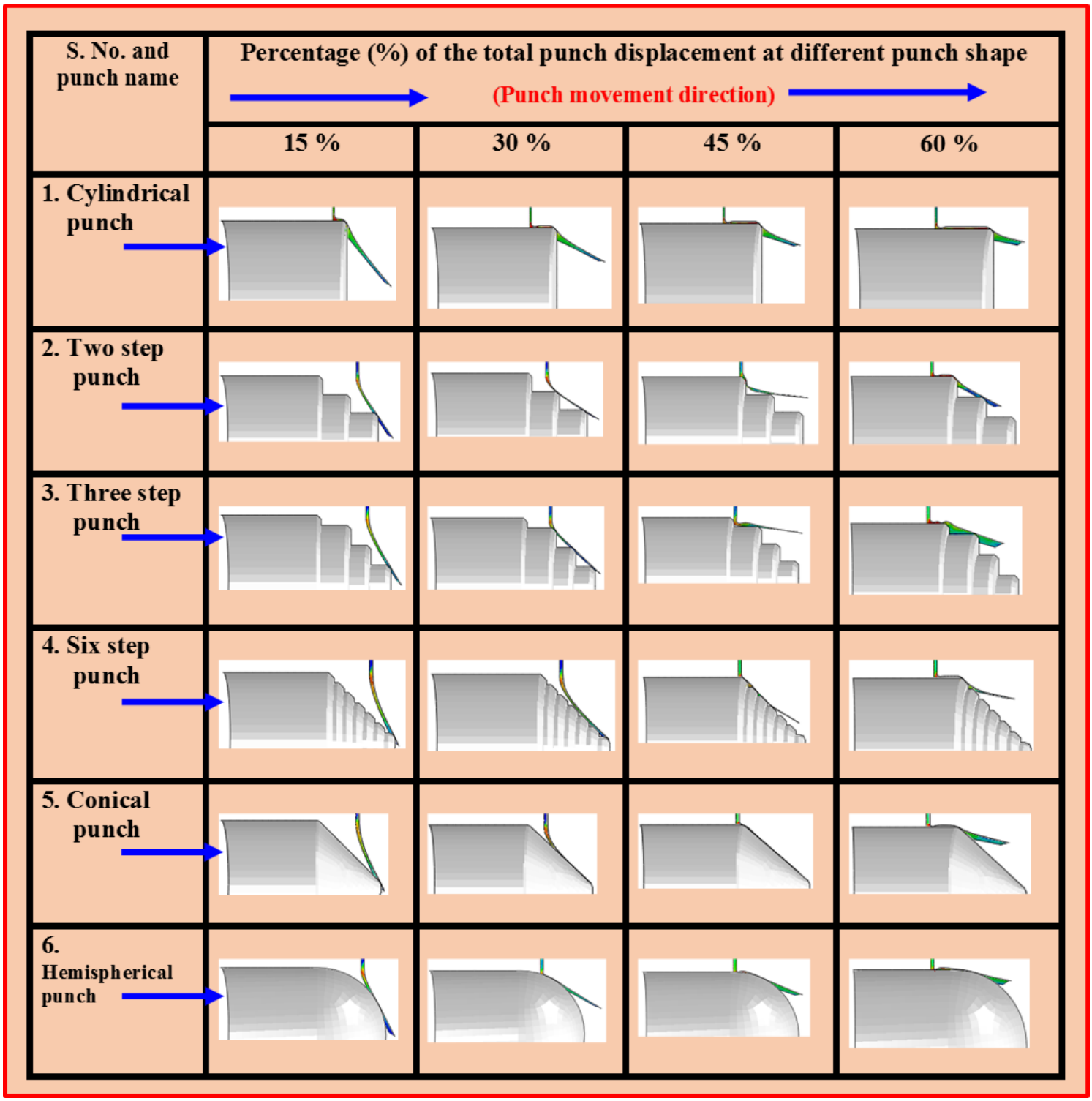

Figure 8

Contact of sheet with different punch shape at various percentage of punch displacement

S. No. and different punch profile with tool set-up	Simulation (Half section view)	Zoom portion	Experimental (Half section view)	Zoom portion
1. Cylindrical 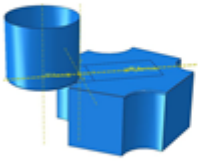	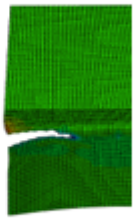	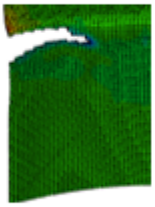		
2. Conical 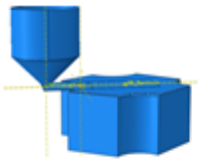	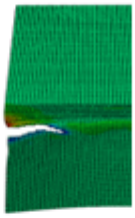	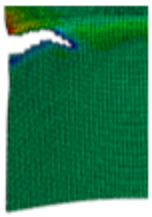		
3. Hemispherical 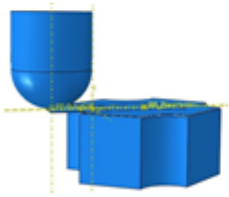	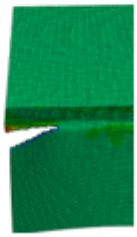	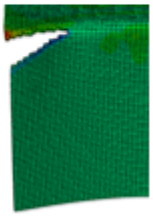		

Figure 9

Assessment of location of crack and its propagation in blank for cylindrical, conical and hemispherical punch using simulation and experimental

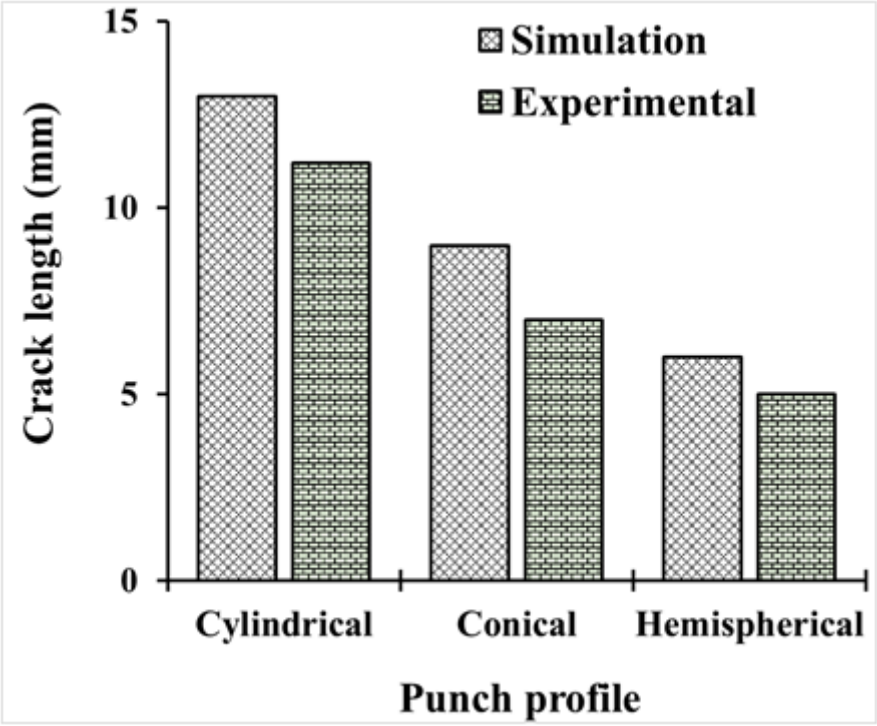

Figure 10

Assessment of length of crack in cylindrical, conical and hemispherical punch using simulation and experimental

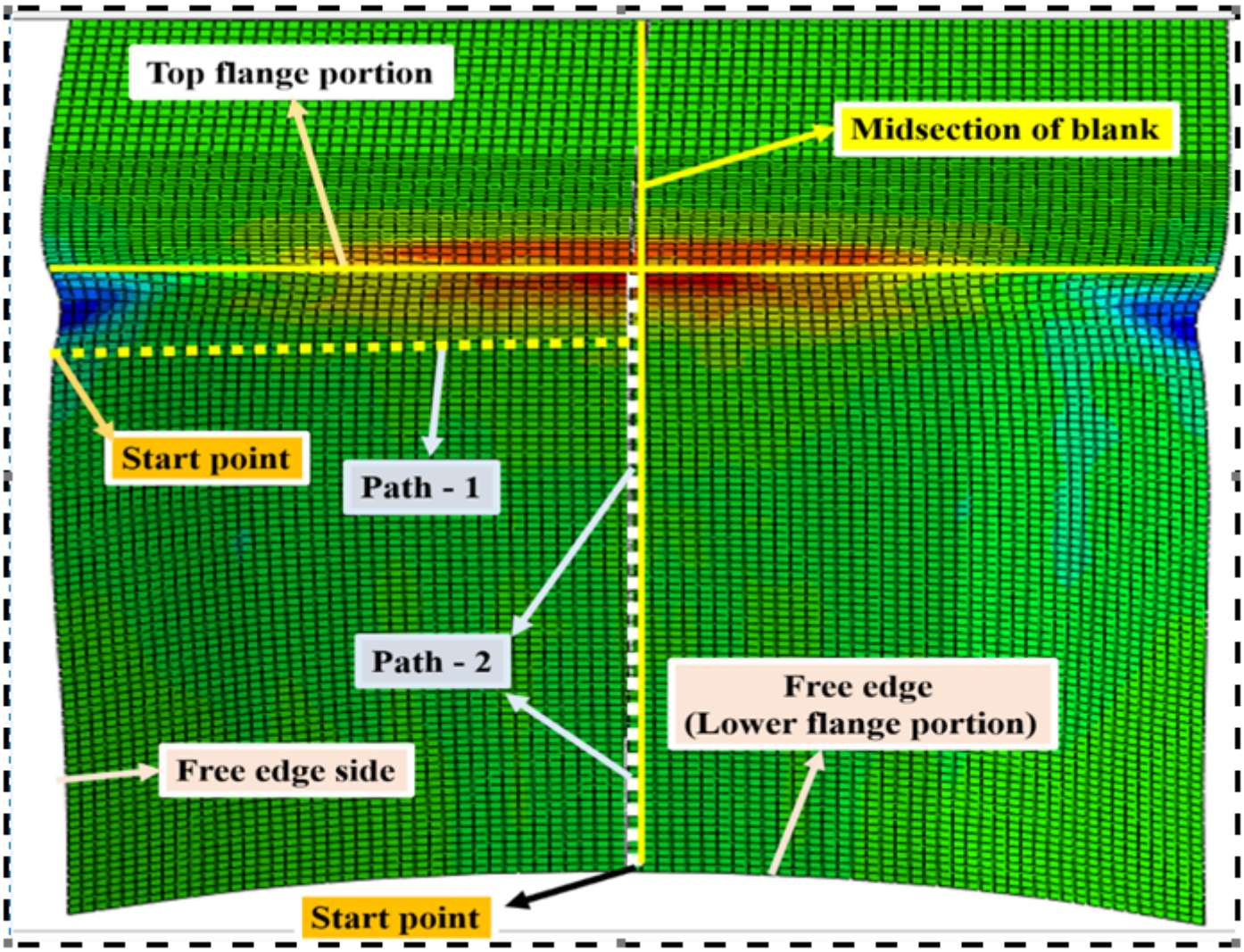

Figure 11

Path-1 and 2, assumed for measuring the blank thickness

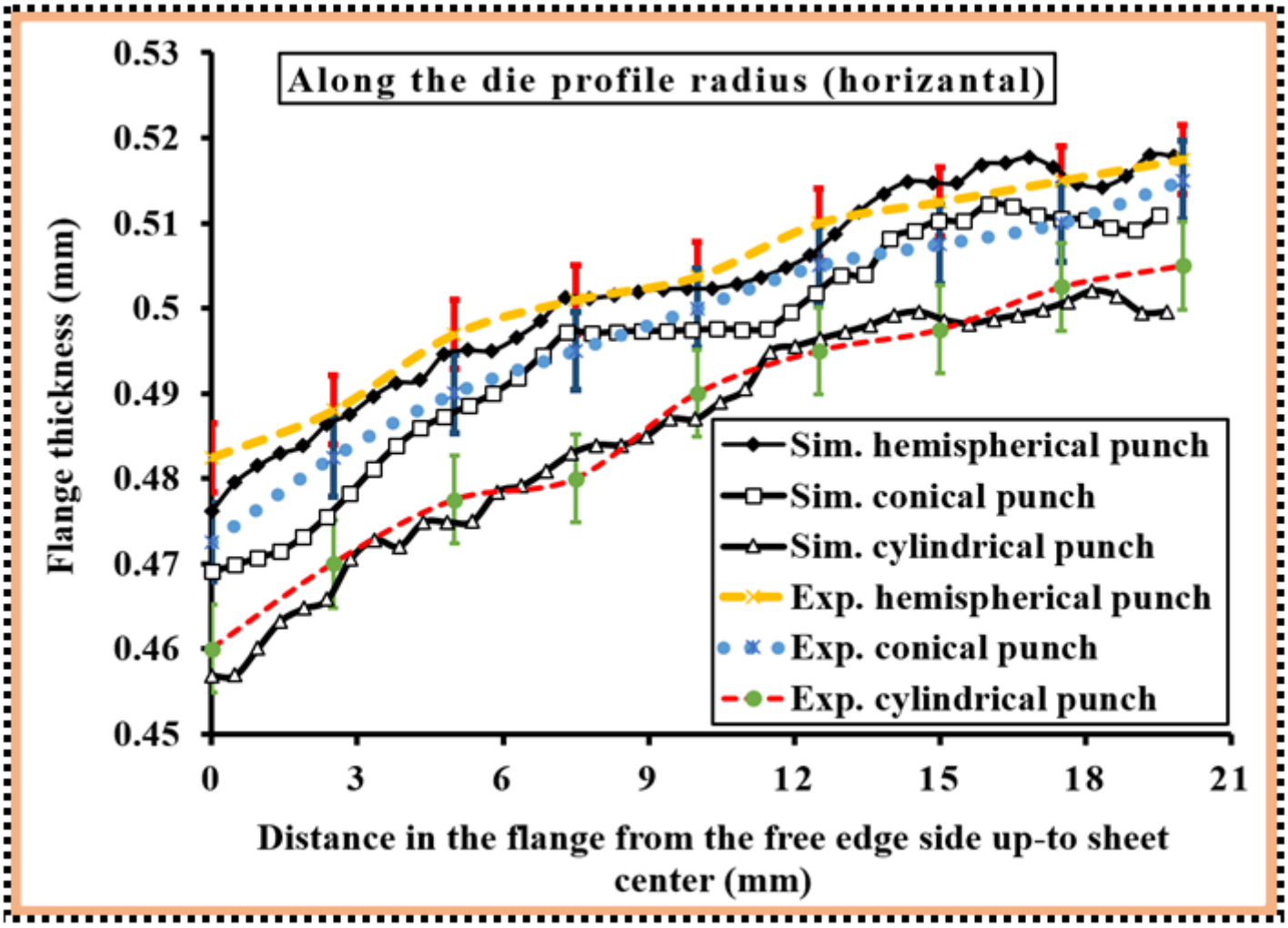

Figure 12

Comparison of thickness distribution on three punch profile (path-1)

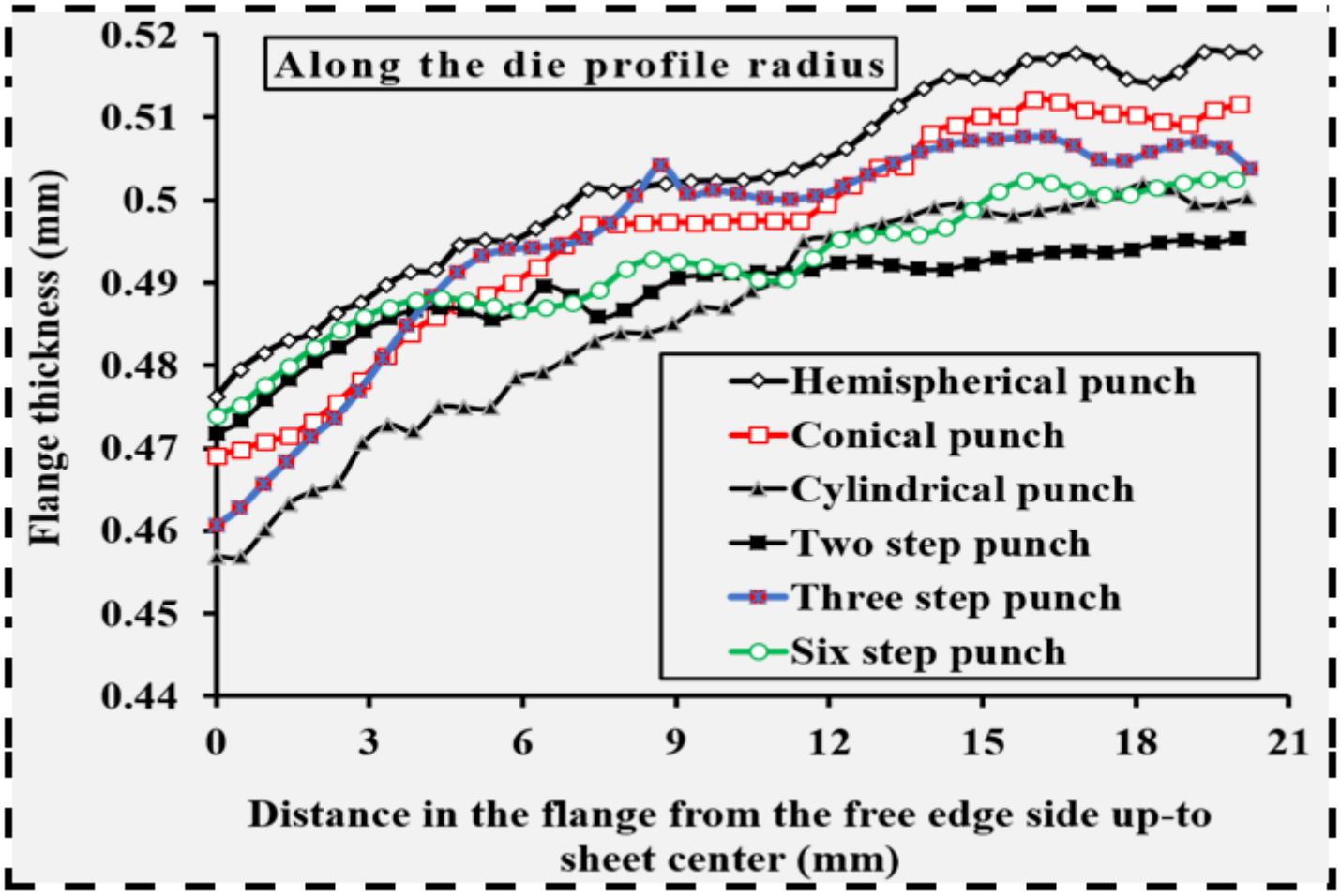

Figure 13

Thickness distribution on different punch profile (path-1)

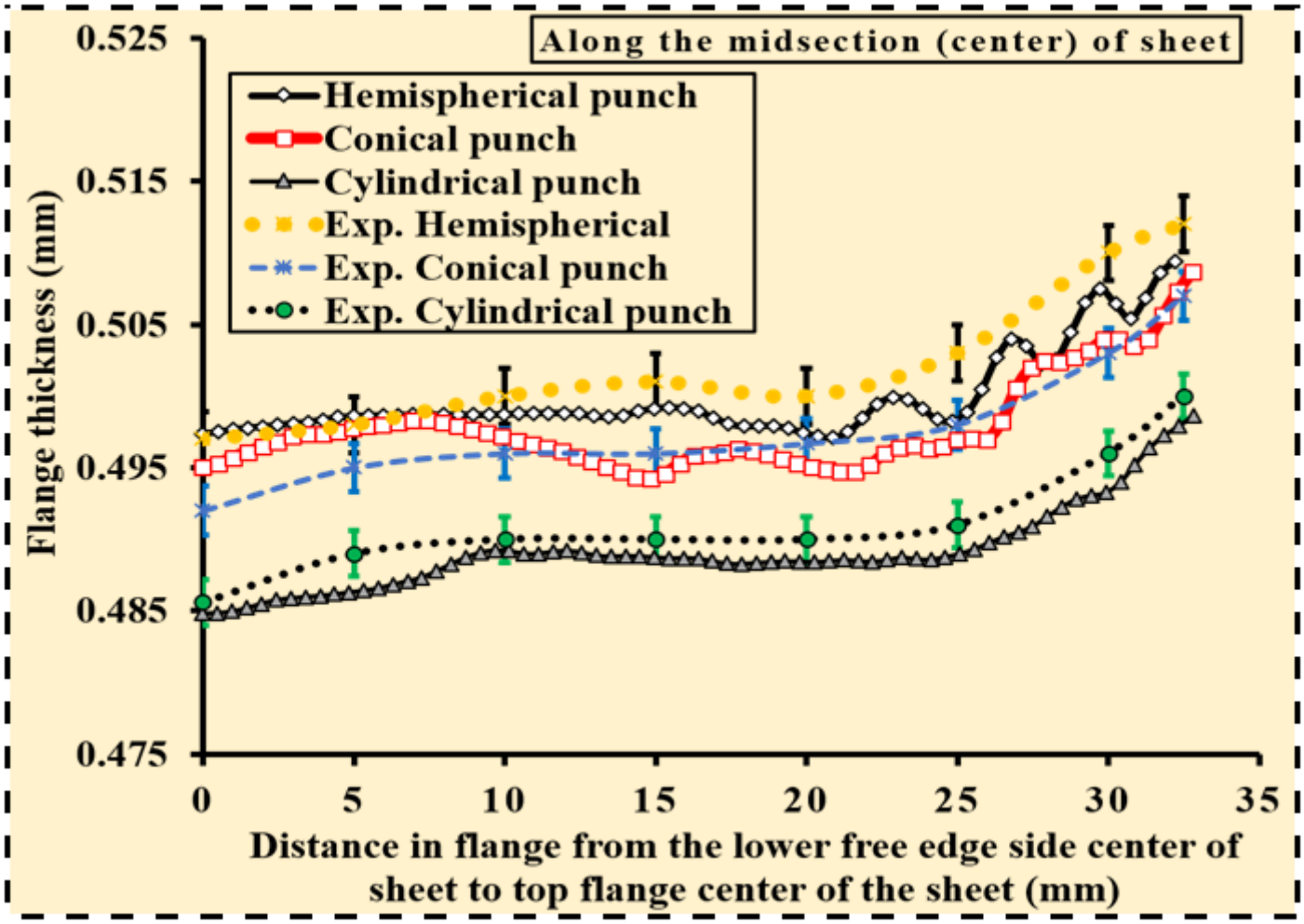

Figure 14

Comparison of thickness distribution on three punch profile, along the midsection of sheet and path–2

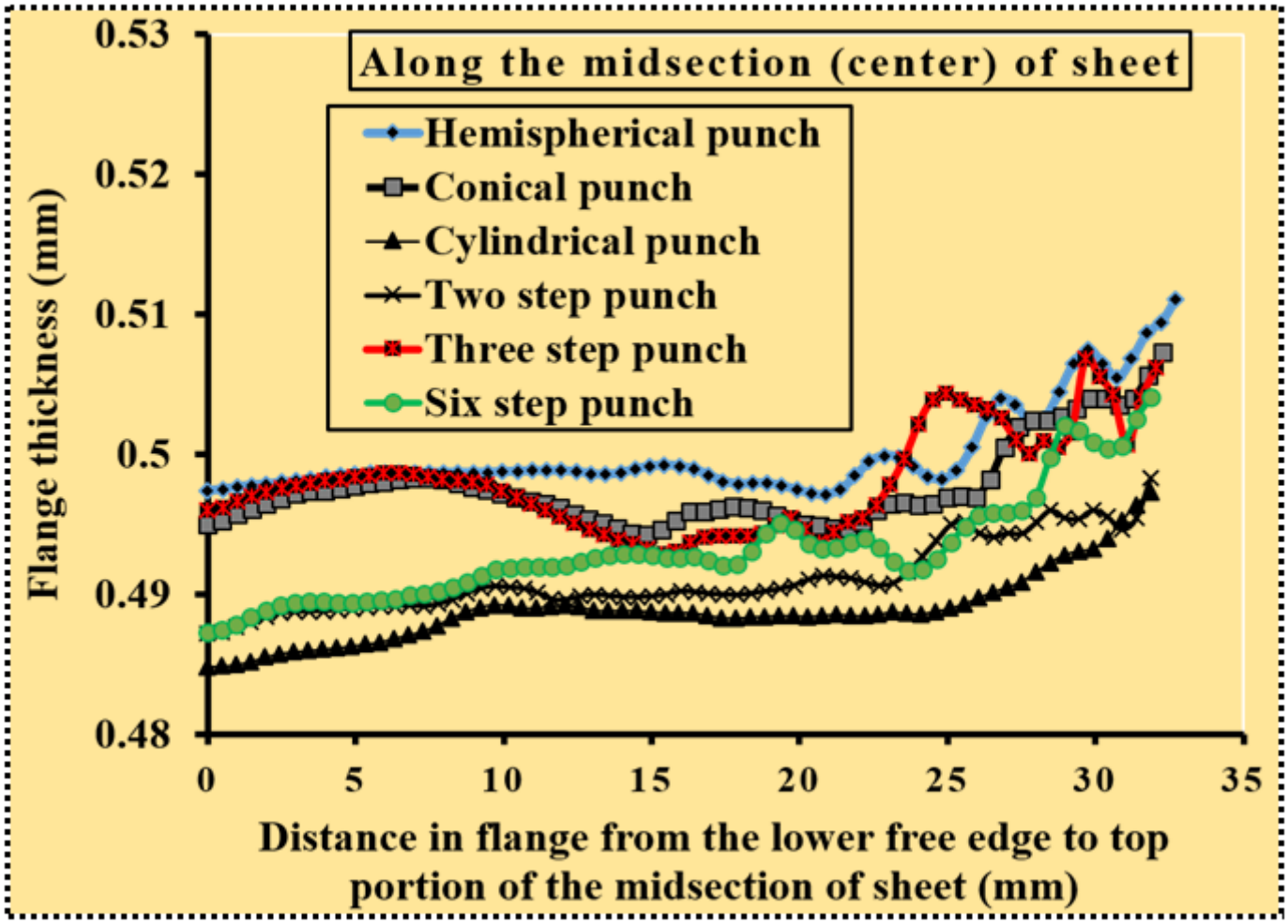

Figure 15

Thickness distribution on different punch profile, along the midsection of sheet and path – 2

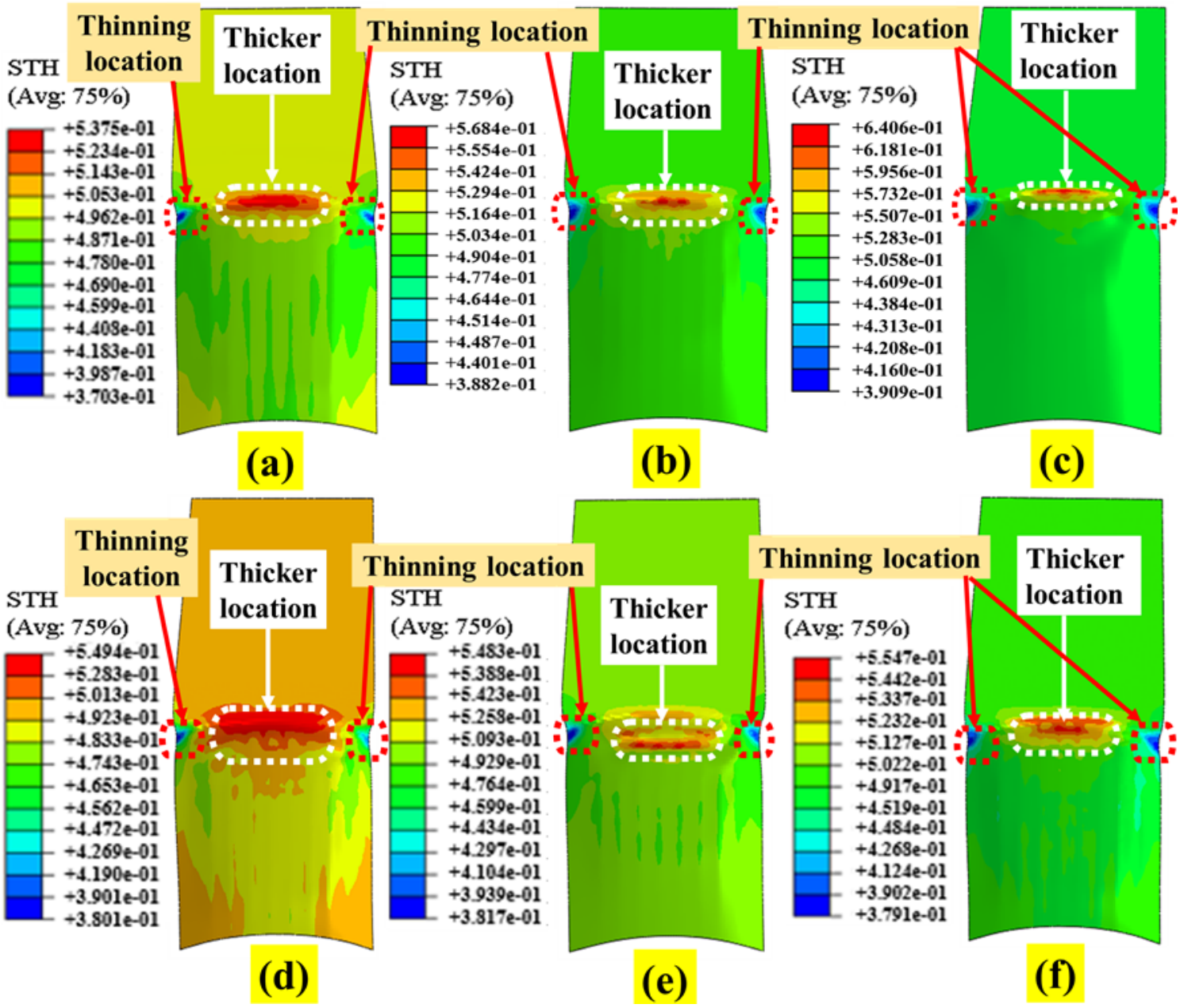

Figure 16

Contour plots for blank thickness variation for various geometry of punch by FE simulation at 1 mm gap between punch and die (a) Cylindrical, (b) Conical, (c) Hemispherical, (d) Two step, (e) Three step and (f) Six step punch

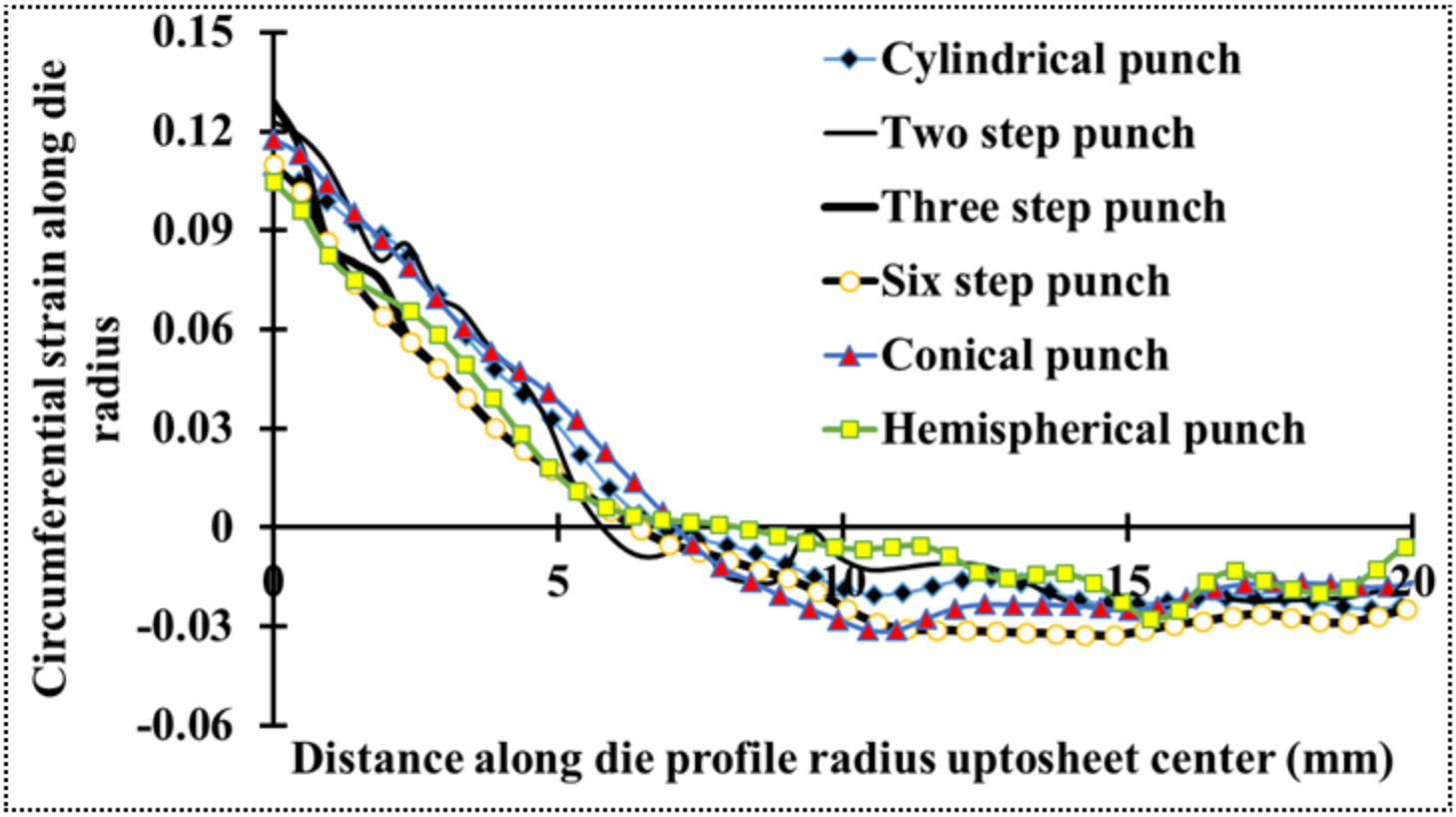

Figure 17

Effect of various geometries of punch on circumferential strain (Path – 1)

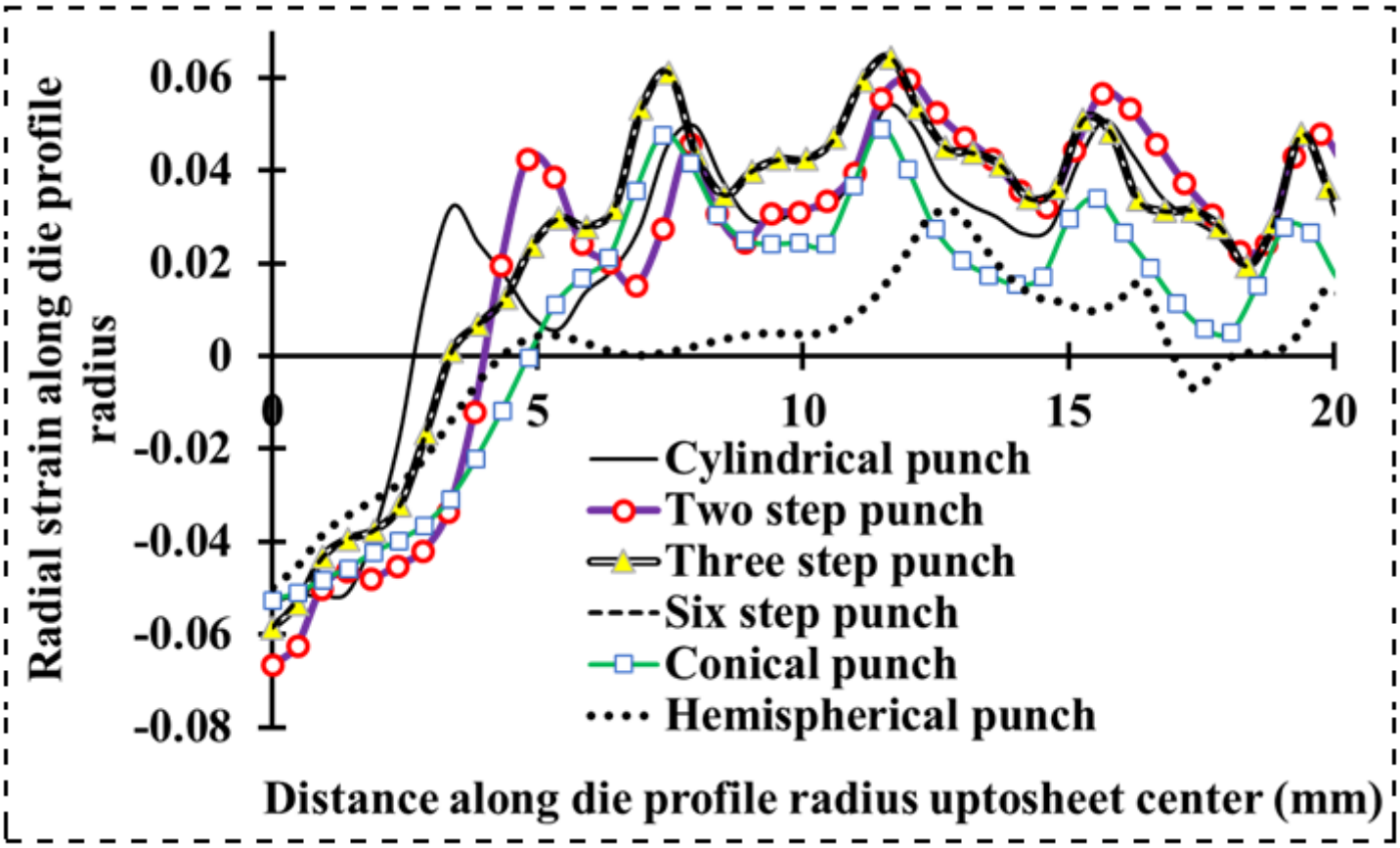

Figure 18

Effect of various geometries of punch on radial strain (Path – 1)

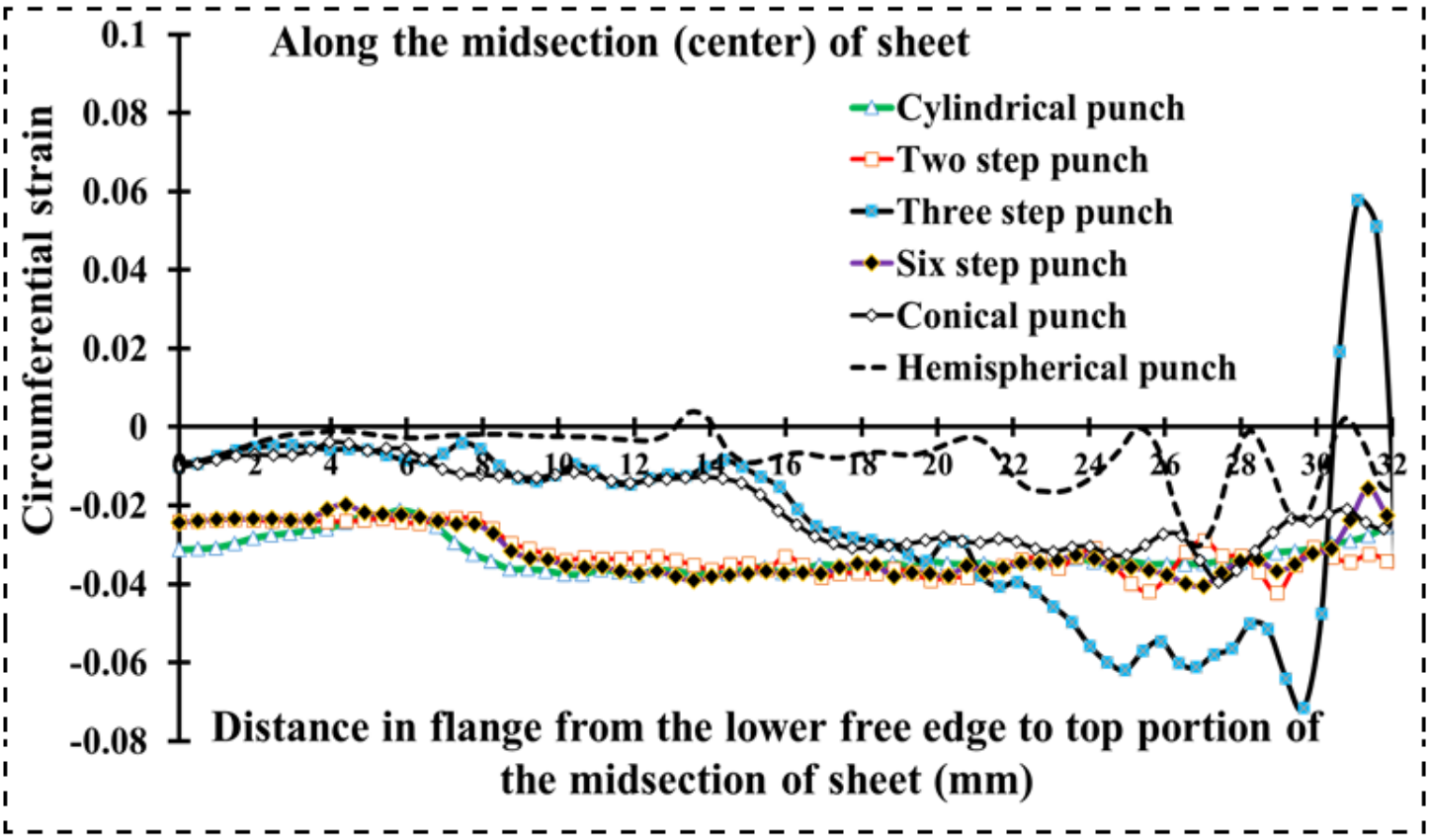

Figure 19

Effect of various geometries of punch on circumferential strain (Path – 2)

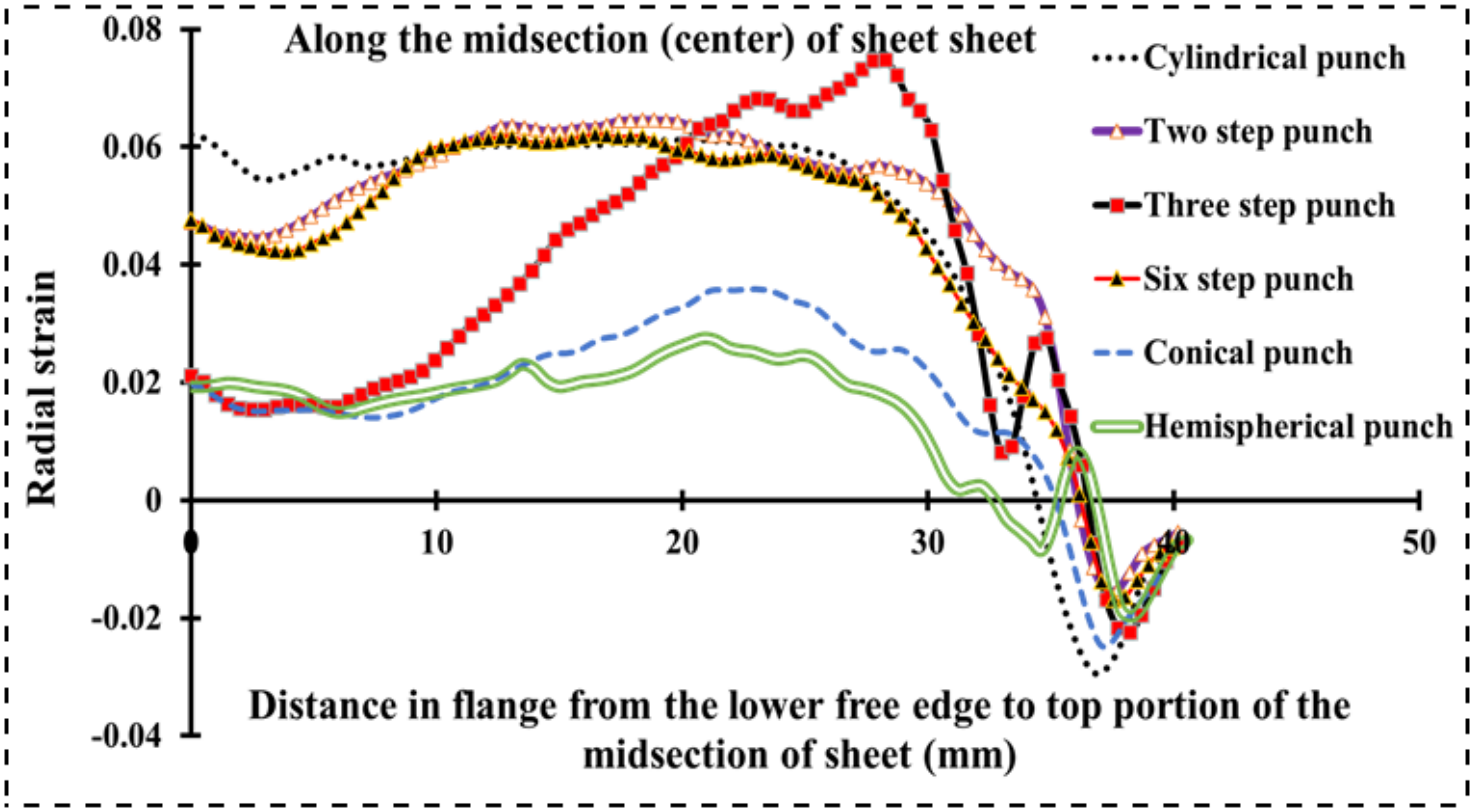

Figure 20

Effect of various geometries of punch on radial strain (Path – 2)

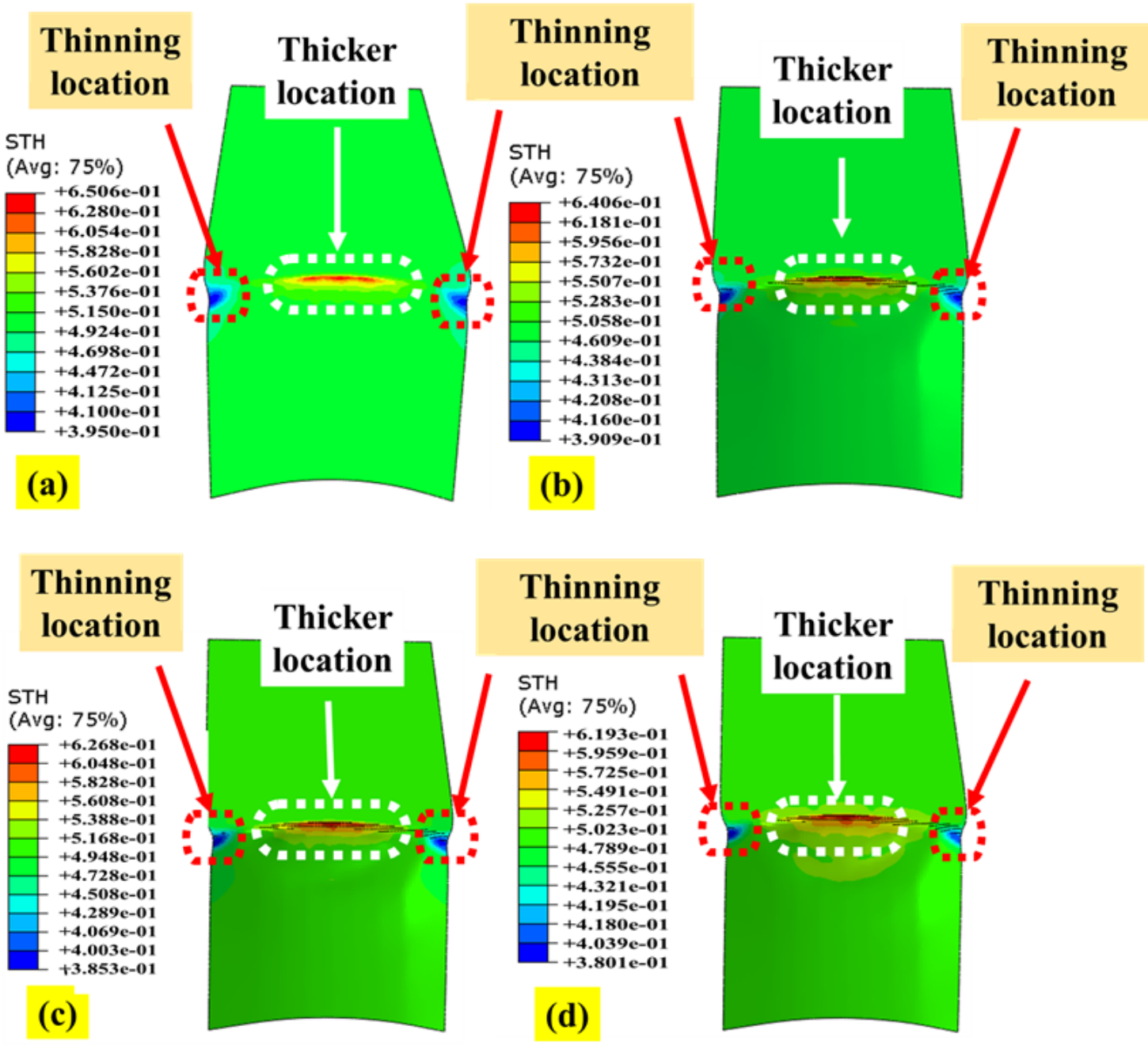

Figure 21

Contour plots for blank thickness variation for hemispherical punch profile and different coefficient of friction by FE simulation at 1 mm gap between punch and die **(a)** μ = 0.05, **(b)** μ = 0.10, **(c)** μ = 0.15 and **(d)** μ = 0.20